Geochemistry of Neogene Siwalik mudstones along Punjab re-entrant, India: Implications for source-area weathering, provenance and tectonic setting

Subhajit Sinha*, R. Islam, Sumit K. Ghosh, Rohtash Kumar and S. J. Sangode

Sedimentology Group, Wadia Institute of Himalayan Geology, Dehra Dun 248 001, India

Mudstones from the Neogene Siwalik succession, east of Ravi River, Punjab re-entrant have been analysed for major, trace and rare earth elements (REEs) used as a reliable proxy to evaluate lithological composition, source-area weathering, provenance and tectonic setting of the basin. Chemical Index of Alteration value of 75 (average) indicates moderate to high weathering condition at the source area. Concentration of transition trace elements, e.g. Cr, Ni and Co in the sediments tends to support metamorphic source area. Plot of Th/Sc and Zr/Sc indicates sediment recycling along with addition of zircon from a weathered source, probably low grade metamorphics apart from first cycle grains from igneous acidic sources. Positive correlation between Al_2O_3 and Fe_2O_3, TiO_2, MgO, K_2O, P_2O_5 is evident. High correlation coefficient between Al_2O_3 and K_2O suggests clay mineral control on the major oxides. Higher concentration of ΣREE and Zr in the sediments suggests heavy minerals as host for the REEs. Chondrite-normalized REE patterns, negative Eu anomaly (Eu/Eu* = 0.61–0.75), ratios of (La_N/Sm_N) = 3.35–4.61; (Ce_N/Yb_N) = 7.39–11.83; (La_N/Yb_N) = 9.31–13.91 and (Gd_N/Yb_N) = 1.30–2.08 collectively suggest that the mudstones are LREE enriched and HREE depleted and derived dominantly from felsic igneous rock and/or reworked metasedimentary/sedimentary source. The geochemical behaviour of the Siwalik mudstones indicates that they are largely derived from a mixed source of granite-gneiss, basic, metamorphic and sedimentary terrain, although upper continental crustal source rocks remained dominant.

Keywords: Chemical Index of Alteration, mudstones, Punjab re-entrant, Siwalik Group.

THE Siwalik Group constitutes an extensive belt of Cenozoic freshwater sediments flanking the southernmost fringe of the Himalaya, and forming the outermost range of the Himalayan chain[1]. The fluvial nature of these clastic sediments is abundantly clear from the sedimentary organization of channel facies (sandstones) and interbedded floodplain facies (mudstone/shale/siltstone). It has been well established that the Siwalik basin received sediments from the adjacent elevated fold-thrust belt (Lesser and Higher Himalaya) and its systematic unroofing history has been recorded along with the basin subsidence and nature of sediment dispersal across the basin. Although sedimentation patterns, granulometric, petrography analysis, and other related studies of these rocks have been carried out in detail[2–8], geochemical investigations of Siwalik mudstones and their implications for source rock, sedimentological processes and tectonic setting have not been attempted so far.

Major, trace and rare earth element (REE) geochemistry has been found to be useful to characterize source-rock weathering, and climatic variability from the terrestrial detritus of the basin[9–11]. Their records are influenced by source-rock lithologies, chemical weathering, sorting, sedimentation and post-depositional diagenetic reactions[12]. Thus distribution of these elements provides clues of the geological processes, provenance and tectonic setting[12–14]. The REE geochemistry has an added advantage over major and trace elements to decipher the provenance, since the concentration of these elements is not affected during erosion, sedimentation and diagenesis, and thus represents a homogenized average source composition[14–16]. This article attempts to understand the tectono-climatic history of the fold-thrust belt using geochemistry of mudstone in the Siwalik succession.

Location and geology

The study area is located east of the Ravi River, Punjab re-entrant in Gurdaspur District, Punjab (Figure 1)[8]. A total 2740 m thick section is measured along Katilu Khad (lat. 32°24′ and long. 75°53′), north of the Jawalamukhi Thrust. It comprises sandstone–mudstone of the upper part of Lower Siwalik (0–500 m), sandstone–mudstone-conglomerate of Middle Siwalik (500–2000 m) and thickly bedded conglomerate of the lower part of Upper Siwalik. This succession is overlain by Lower Tertiary sedimentary rocks with thrust contact (splay of the Main Boundary Thrust; MBT) towards the north (Figure 1).

*For correspondence. (e-mail: sinha_subho@rediffmail.com)

The northerly disposed fold-thrust belt has complicated tectonostratigraphic relationships between the thrusts and the various stratigraphic units. The major thrusts from south to north are MBT and Chail Thrust (CT ≈ Panjal Thrust). The Lesser Himalayan formations, also known as the Panjal Imbricate Zone (PIZ), are delimited by CT in the north and MBT towards the south[17]. The PIZ contains Mandi-Darla basic volcanics with intercalations of quartzite. The Mandi-Darla basic volcanics succession is tectonically overlain by phyllite, slate and limestone. North of

Figure 1. *a*, Simplified geologic map of the Himalaya showing the location of the study area in regional context. *b*, Detailed geological map of the study area and its hinterland along Ravi River, NW part of Himalaya[8].

CT lies the Chamba Group of rocks and Dhauladhar granites and gneisses[17] (Figure 1). The Chamba Group of rocks consist of slate, meta-siltstone, meta-greywacke, quartzite, green and grey phyllite, phyllitic quartzite, micaceous quartzite and occasional bands of grey marble and volcanic layers together with biotite and garnet–biotite schist. The Dhauladhar massif comprises foliated muscovite and boitite-bearing granite gneiss with Rb–Sr whole-rock isochron age[18–21] of 500–450 Ma. A narrow stretch of mylonite augen gneiss sandwiched between the Dhauladhar granites and rocks of Chamba Group extends >200 km along the regional strike. In the Baragaon area of Satluj valley, the mylonitic augen gneiss is dated[21] as 1430 ± 150 Ma.

Sampling and analytical methods

Mudstone samples were collected from the Lower and Middle Siwalik succession exposed in the Katilu Khad section (~2000 m). Adequate care was taken to choose samples only from non-pedogenic mudstone horizons. Majority of the 51 mudstone samples are purple, while few are grey. The rock chips were powdered using TEMA swing mill to –200 μm mesh size. The major and trace elements were analysed by Wave Length Dispersive XRF system (Siemens SRS 3000) at WIHG, Dehra Dun. Analysis was carried out using pressed powder pellets glued with polyvinyl alcohol. The analytical procedure followed was as given by Lucas-Tooth and Pyne[22].

REE was measured by Inductively Coupled Plasma-Mass Spectrometry (ICP-MS; Perkin Elmer) at WIHG, with 0.04 g of the sample subjected to standard acid digestion with HF–HNO$_3$. The standard acid treatment was repeated until a clear solution was obtained. The clear solution was then treated with 1 N HNO$_3$ and 100 ml solution was obtained, which was ready for analysis. The accuracy and precision was ±1–3% for major oxides, and for trace and REEs ±5–10%. Chemical data are present in Tables 1–3.

Geochemistry

Major elements

The major element composition of the Katilu Khad mudstones is quite variable. SiO$_2$ range from 49.26 to 87.52 wt%, whereas Al$_2$O$_3$ varies from 7.38 to 21.92 wt%. The behaviour indicates linear negative array of different major elements (Al$_2$O$_3$, Fe$_2$O$_3$, MgO and K$_2$O) against SiO$_2$, scattered distribution in case of CaO and Na$_2$O, and a fairly good correlation between SiO$_2$ and TiO$_2$ (Figure 2 *a*). However, TiO$_2$, Fe$_2$O$_3$, MgO and K$_2$O exhibit positive correlation with Al$_2$O$_3$ (Figure 2 *b*). The higher correlation coefficient between Al$_2$O$_3$ and K$_2$O (r = 0.92) indicates clay mineral control on the major element composition of the mudstones. CaO exhibits almost similar
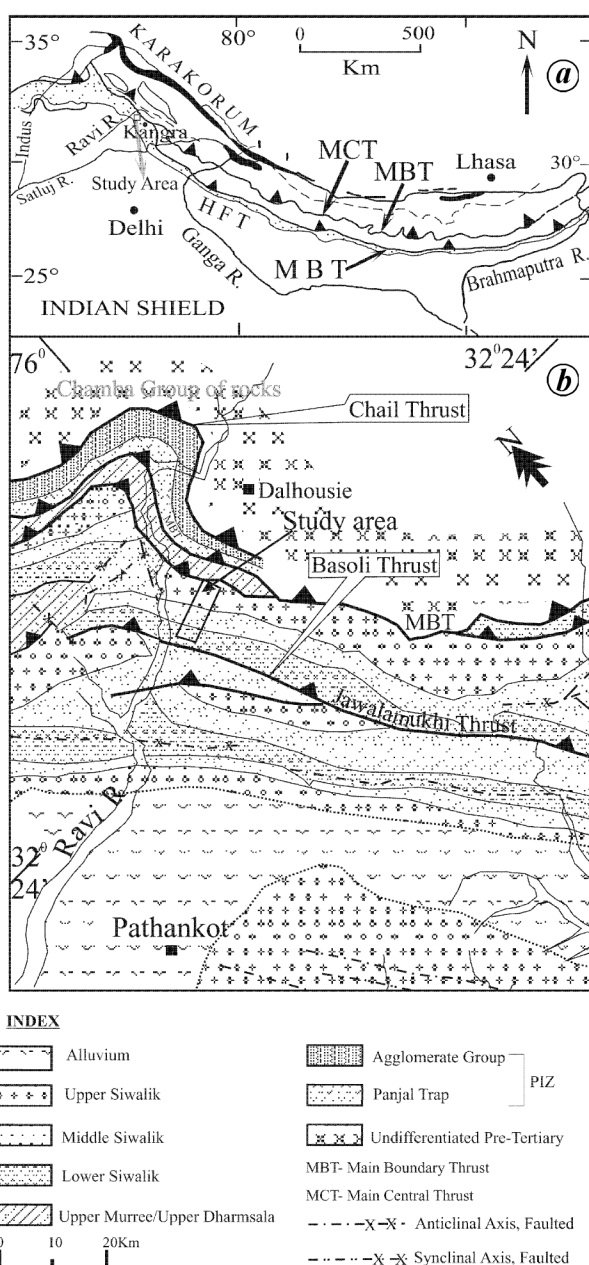
Table 1. Major element composition of mudstones of Katilu Khad section

Sample no.	SH (m)	SiO_2	TiO_2	Al_2O_3	Fe_2O_3	MnO	MgO	CaO	Na_2O	K_2O	P_2O_5	LOI
KKC1	37	62.26	0.73	17.44	6.75	0.05	3.53	1.56	0.75	3.45	0.09	4.24
KKC2	51	66.35	0.81	16.66	6.15	0.05	2.96	0.33	0.63	3.06	0.05	2.99
KKC3	61	71.63	0.83	14.12	5.64	0.06	2.14	0.44	0.86	2.13	0.05	4.90
KKC4	76	73.32	0.78	13.58	5.41	0.06	2.15	0.78	0.88	2.08	0.06	2.13
KKC5	97	78.12	0.61	12.20	4.37	0.05	1.89	0.24	0.75	1.84	0.05	1.08
KKC6	126	63.23	0.74	16.81	7.40	0.06	2.70	0.52	0.96	2.94	0.13	4.99
KKC7	237	71.05	0.69	14.09	4.77	0.05	2.32	1.68	0.63	2.28	0.09	1.59
KKC8	271	67.66	0.71	16.65	7.07	0.07	2.13	0.27	0.65	2.95	0.07	2.70
KKC9	292	63.00	0.71	18.59	6.21	0.05	2.56	1.29	0.48	3.60	0.08	6.86
KKC10	327	65.58	0.74	17.57	6.59	0.07	2.30	1.15	0.45	3.12	0.07	3.44
KKC11	342	59.98	0.74	20.48	7.43	0.06	2.59	0.74	0.59	4.14	0.10	3.45
KKC12	377	56.68	0.68	21.92	7.31	0.06	2.63	1.22	0.33	4.88	0.09	6.45
KKC13	399	56.06	0.71	15.30	6.05	0.06	4.30	5.20	0.95	2.63	0.12	10.31
KKC14	432	65.93	0.77	17.70	5.32	0.04	3.00	0.46	0.60	3.21	0.07	2.99
KKC15	463	58.41	0.79	19.80	7.89	0.05	3.10	1.22	0.42	3.88	0.09	5.04
KKC16	480	62.47	0.78	17.62	6.42	0.05	3.36	0.65	0.82	3.48	0.11	3.85
KKC17	497	62.08	0.76	17.65	6.35	0.05	3.34	0.65	0.79	3.47	0.12	3.85
KKC18	537	60.90	0.72	17.48	6.75	0.07	2.97	1.89	0.72	3.84	0.13	5.83
KKC19	562	66.11	0.81	17.25	6.91	0.05	2.30	0.46	0.37	3.38	0.10	3.40
KKC20	573	67.14	0.75	16.01	5.65	0.04	2.39	0.55	0.49	2.91	0.08	3.49
KKC21	600	55.73	0.78	17.07	7.25	0.11	2.96	3.92	0.50	3.59	0.11	9.58
KKC22	617	75.64	0.75	13.17	5.20	0.05	1.82	0.22	0.60	2.05	0.08	4.00
KKC23	630	69.16	0.74	16.34	5.27	0.04	2.14	0.19	0.85	2.70	0.05	4.00
KKC24	639	79.76	0.57	10.07	3.65	0.08	1.55	1.59	0.93	1.61	0.08	4.78
KKC25	657	56.18	0.75	17.49	7.63	0.08	3.93	2.05	1.03	4.04	0.12	9.34
KKC26	670	71.48	0.77	14.78	5.50	0.04	2.36	0.55	0.48	2.41	0.07	5.42
KKC27	671	63.00	0.69	13.16	5.23	0.11	2.52	5.52	0.51	2.17	0.09	9.50
KKC28	760	60.61	0.74	15.07	5.74	0.16	2.86	4.75	0.58	2.91	0.10	10.73
KKC29	810	61.44	0.72	16.87	6.66	0.08	2.65	1.96	0.73	3.46	0.10	7.52
KKC30	866	63.26	0.71	14.79	5.74	0.05	3.18	2.88	1.15	2.93	0.13	7.23
KKC31	876	59.34	0.71	14.99	5.28	0.07	3.56	3.94	0.91	3.05	0.12	8.90
KKC32	908	58.12	0.77	20.31	7.99	0.05	2.61	0.60	0.37	4.87	0.10	8.03
KKC33	959	54.40	0.67	14.98	5.39	0.14	3.18	6.17	0.93	3.06	0.12	10.72
KKC34	995	58.21	0.82	17.59	7.55	0.14	3.00	3.12	0.38	3.54	0.13	8.47
KKC35	1017	65.40	0.76	15.90	5.62	0.06	2.93	1.10	0.73	2.98	0.10	6.34
KKC36	1103	65.99	0.69	15.09	5.51	0.06	2.56	2.35	0.91	3.01	0.10	3.86
KKC37	1171	55.87	0.83	18.72	7.66	0.06	3.48	2.12	0.42	3.91	0.12	7.20
KKC38	1221	60.53	0.75	16.70	6.73	0.08	2.85	2.74	0.72	3.52	0.10	9.13
KKC39	1234	49.26	0.63	14.87	5.36	0.14	2.87	1.00	0.44	3.07	0.12	18.84
KKC40	1241	62.53	0.85	17.17	7.35	0.05	2.72	1.46	0.63	3.59	0.10	3.74
KKC41	1278	73.19	0.79	13.56	5.80	0.05	2.35	0.24	0.62	2.08	0.06	1.38
KKC42	1284	68.54	0.93	16.19	6.66	0.04	2.35	0.36	0.47	2.73	0.06	4.22
KKC43	1345	64.65	0.59	14.41	5.68	0.08	2.41	3.52	0.86	2.92	0.11	3.90
KKC44	1411	73.87	0.69	13.65	5.04	0.04	2.08	0.48	1.02	2.77	0.08	2.04
KKC45	1431	87.52	0.57	7.38	1.43	0.03	0.86	0.23	0.61	0.90	0.04	1.48
KKC46	1457	62.49	0.82	16.23	6.93	0.09	2.76	2.69	0.48	3.25	0.14	3.99
KKC47	1491	83.08	0.62	9.47	3.37	0.04	1.12	0.25	0.32	1.50	0.06	1.86
KKC48	1530	74.26	0.59	13.74	4.69	0.04	1.57	0.48	0.93	3.28	0.08	2.26
KKC49	1574	69.85	0.72	14.08	4.79	0.06	2.12	2.20	0.50	2.83	0.10	2.66
KKC52	1754	66.49	0.72	17.82	6.76	0.05	2.06	0.49	0.17	3.62	0.08	2.18
KKC56	1996	66.28	0.72	17.70	6.27	0.10	2.03	1.05	0.19	3.29	0.08	3.70

SH, Stratigraphic height; LOI, Loss-on-ignition.

type of behaviour for both SiO_2 and Al_2O_3 (a wide scatter). Major oxides are normalized with Post-Archean Australian Shale (PAAS) value[23] (Figure 3), which indicates enrichment of Al_2O_3, Fe_2O_3 and MgO, slight enrichment of SiO_2, and depletion of TiO_2, Na_2O and P_2O_5; this suggests a mixed provenance. The striking variations of CaO and depletion of Na_2O compared to PAAS reflect moderate to strong weathering, recycling of the source rock, and their removal and addition during transportation.

In the Al_2O_3 versus K_2O plot, mudstone samples plot close to the illite line, suggesting that major K_2O- and Al_2O_3-bearing minerals in the samples are illite (Figure 2 b). High concentrations of Al_2O_3 and K_2O in few sam-

Table 2. Trace element composition of mudstones of Katilu Khad section

Sample no.	SH (m)	Ba	Cr	V	Sc	Co	Ni	Cu	Zn	Ga	Pb	Th	Rb	U	Sr	Y	Zr	Nb
KKC1	37	478	154	117	16	19	58	28	91	18	19	15	163	4	98	30	174	15
KKC2	51	462	179	106	17	19	56	33	86	16	26	15	152	4	76	38	265	16
KKC3	61	348	225	109	10	17	56	27	71	14	22	15	103	3	57	36	329	16
KKC4	76	345	236	106	13	16	40	26	71	13	22	16	102	1	59	36	299	16
KKC5	97	289	218	74	10	14	40	24	64	11	15	11	88	2	56	31	238	13
KKC6	126	422	158	126	15	21	66	51	86	17	27	15	145	3	79	27	195	14
KKC7	237	372	157	87	10	14	53	30	71	13	21	14	104	3	64	37	274	14
KKC8	271	608	109	104	12	17	42	32	87	18	33	16	141	5	65	39	214	15
KKC9	292	638	112	114	14	17	51	26	91	19	25	16	170	4	92	38	215	15
KKC10	327	549	115	105	11	17	53	28	87	17	27	16	154	4	71	39	220	16
KKC11	342	754	102	127	15	19	57	34	108	22	30	17	203	4	103	35	183	16
KKC12	377	714	103	130	18	20	55	32	108	23	31	18	223	3	82	34	164	15
KKC13	399	402	116	107	16	18	53	36	83	15	23	12	111	5	128	30	177	14
KKC14	432	489	184	104	19	13	41	32	70	12	18	9	98	3	109	25	102	10
KKC15	463	607	131	133	13	18	74	41	93	16	22	14	150	3	96	30	239	15
KKC16	480	509	137	110	16	25	86	40	108	22	33	17	195	4	108	34	179	16
KKC17	497	499	137	108	17	21	64	42	99	18	25	16	171	4	93	31	207	17
KKC18	537	590	98	112	19	19	58	34	103	21	28	15	172	3	70	37	175	14
KKC19	562	590	102	115	17	20	63	30	101	21	27	17	166	1	68	42	209	16
KKC20	573	540	124	110	14	15	57	31	86	18	22	14	139	3	99	37	271	15
KKC21	600	567	113	121	19	20	88	34	97	21	29	15	151	2	129	31	158	13
KKC22	617	397	164	90	11	15	50	27	72	15	23	13	101	3	70	36	376	17
KKC23	630	556	142	101	14	15	51	27	74	17	22	16	135	4	92	38	286	15
KKC24	639	232	247	70	9	10	37	24	57	11	15	10	74	3	63	33	289	12
KKC25	657	693	104	117	16	20	65	42	108	22	32	14	196	3	103	32	131	15
KKC26	670	389	181	103	13	15	66	30	74	16	22	15	108	4	64	35	414	16
KKC27	671	261	163	93	17	16	72	27	73	14	16	11	91	3	84	32	217	13
KKC28	760	516	90	104	20	15	58	27	80	16	26	12	123	3	107	35	190	13
KKC29	810	564	181	111	14	18	47	31	95	19	27	15	149	3	84	37	194	14
KKC30	866	532	125	100	15	17	37	33	84	17	24	13	118	4	97	36	228	14
KKC31	876	484	105	103	18	15	39	33	84	16	27	13	120	4	79	35	236	15
KKC32	908	738	101	133	20	20	62	31	115	27	31	18	218	3	88	37	166	15
KKC33	959	489	80	97	18	16	38	29	81	16	23	12	132	3	109	32	163	14
KKC34	995	462	143	130	16	20	94	32	102	22	26	15	156	2	93	40	168	14
KKC35	1017	353	332	112	17	19	78	33	85	17	25	13	135	3	109	30	227	14
KKC36	1103	454	114	101	16	14	47	31	84	16	23	13	127	3	88	37	230	14
KKC37	1171	547	164	131	17	21	107	34	106	22	28	13	168	3	150	33	171	15
KKC38	1221	548	104	116	16	18	71	38	98	21	26	14	157	3	114	35	178	14
KKC39	1234	372	113	115	20	15	65	29	80	15	21	10	115	2	172	28	122	10
KKC40	1241	567	111	136	20	20	76	31	104	23	27	16	170	2	114	38	185	16
KKC41	1278	323	196	111	12	18	79	30	75	15	20	14	104	3	77	34	373	17
KKC42	1284	425	184	133	16	18	78	33	92	19	27	16	146	3	103	32	268	18
KKC43	1345	418	107	130	15	15	57	30	86	17	23	12	137	2	114	34	187	13
KKC44	1411	379	178	141	11	14	50	27	74	15	22	15	131	2	69	37	341	14
KKC45	1431	150	308	108	7	6	25	19	49	8	14	10	55	4	35	37	468	14
KKC46	1457	434	114	283	18	19	81	29	93	19	26	16	152	3	84	39	183	15
KKC47	1491	205	307	259	8	10	29	19	60	11	18	11	86	2	30	37	420	14
KKC48	1530	386	150	271	11	11	26	24	73	14	21	16	150	2	53	41	322	13
KKC49	1574	388	108	289	17	13	53	31	79	16	24	14	140	3	91	39	231	14
KKC52	1754	571	91	316	13	18	49	31	102	22	25	16	180	2	54	39	185	14
KKC56	1996	558	109	311	17	17	45	29	94	21	28	17	156	2	52	40	205	15

ples imply that illite is the dominant aluminosilicate. This interpretation is further supported by the low K_2O/Al_2O_3 ratios (average 0.19).

A scattered behaviour observed between Al_2O_3 and Na_2O suggests that mineral phases such as plagioclase do not have major control on the Al_2O_3 content. However, a positive correlation between Al_2O_3 and K_2O indicates the presence of K-feldspar. Although almost all samples plot on the illite line, suggesting decomposition of K-feldspar and muscovite during moderate to intense weathering under humid climate, the potash remained fixed in the clays. This suggests significant contribution from the granite/ granite-gneisses. In general, the total iron content of these rocks is quite high indicating close association of phyllosilicates derived from a biotite-rich source possibly granite and/or phyllite-schist rich provenance.

Table 3. REE data for some selected samples of mudstone deposits of Katilu Khad section

Element	La	Ce	Pr	Nd	Sm	Eu	Gd	Tb	Dy	Ho	Er	Tm	Yb	Lu
KKC1	46.53	93.44	9.52	37.66	7.36	1.42	5.36	0.90	4.87	0.99	2.89	0.44	2.54	0.37
KKC2	48.81	100.95	10.29	42.09	8.11	1.55	6.08	0.99	5.26	1.02	2.96	0.43	2.40	0.36
KKC3	49.78	100.35	10.25	41.85	8.02	1.42	5.94	0.96	4.96	0.97	2.84	0.41	2.46	0.35
KKC4	52.66	109.03	11.24	46.76	8.78	1.56	6.58	1.07	5.46	1.04	2.97	0.44	2.55	0.38
KKC18	52.67	148.55	10.94	27.86	8.88	1.78	6.97	1.11	6.47	1.28	3.86	0.53	3.25	0.50
KKC19	53.87	112.06	11.69	47.95	10.05	2.20	7.97	1.29	7.58	1.50	4.34	0.59	3.76	0.56
KKC20	44.80	89.06	9.12	36.35	6.94	1.39	5.46	0.90	5.28	1.10	3.24	0.46	2.87	0.44
KKC21	48.19	98.10	9.99	39.44	7.77	1.60	6.02	0.97	5.71	1.18	3.52	0.51	3.26	0.49
KKC22	46.96	96.00	9.96	39.95	7.89	1.45	6.11	1.01	6.00	1.23	3.66	0.52	3.27	0.50
KKC23	46.04	93.32	10.26	42.38	8.63	1.69	6.58	1.04	6.11	1.20	3.55	0.48	3.00	0.45
KKC31	43.42	99.39	9.09	32.55	7.39	1.43	5.77	0.86	5.21	1.02	3.04	0.42	2.56	0.40
KKC32	52.88	107.81	10.96	44.09	8.78	1.76	6.91	1.10	6.45	1.30	3.92	0.54	3.48	0.51
KKC33	42.51	84.05	8.79	35.42	7.19	1.40	5.61	0.87	4.97	0.97	2.92	0.39	2.47	0.37
KKC34	49.23	101.88	10.40	42.59	8.66	1.81	7.27	1.19	7.14	1.44	4.19	0.58	3.57	0.54
KKC35	48.13	101.61	10.22	41.28	8.30	1.63	6.24	1.02	5.88	1.18	3.48	0.49	3.10	0.47
KKC36	44.41	89.08	9.19	36.29	7.54	1.44	5.90	0.97	5.67	1.16	3.45	0.50	3.01	0.45
KKC40	49.35	101.85	10.44	42.81	8.56	1.79	6.71	1.16	6.46	1.31	3.83	0.59	3.49	0.54
KKC41	44.35	93.03	9.53	39.05	7.40	1.35	5.54	0.93	5.13	1.05	3.09	0.47	2.77	0.43
KKC42	46.80	94.61	9.52	38.53	6.38	1.14	4.72	0.80	4.56	0.99	3.01	0.47	2.91	0.43
KKC43	42.00	86.79	8.99	36.68	7.50	1.47	5.80	1.01	5.59	1.14	3.28	0.51	3.00	0.44
KKC44	45.64	95.30	9.86	40.80	7.83	1.35	5.89	1.00	5.55	1.12	3.28	0.49	2.89	0.44
KKC45	35.58	72.67	7.63	31.88	6.17	1.13	4.91	0.83	4.60	0.94	2.70	0.40	2.30	0.34

The concentration of CaO is generally modified because of the authigenic nature of the sedimentary carbonate mineral[24]. Since CaO* in the Chemical Index of Alteration (CIA) represents CaO derived only from silicates (essentially plagioclase), all non-silicate CaO must be subtracted. Relationship between CaO and loss-on-ignition (LOI) shows that the former is well correlated with the latter (r = +0.84; Figure 2 b). This implies that the abundance of CaO content in the mudstones probably reflects the abundance of carbonate minerals in the source area. However, CaO vs LOI plots toward higher LOI in the x-axis and probably reflects the presence of other volatile materials (Figure 2 b). A positive correlation of major elements like Fe–Mg oxide with Al_2O_3 indicates a basic rock input. This proves that although some of the CaO is bound to the carbonate fraction, most of the CaO comes from plagioclase derived from a basic rock source. Other major elements are generally concentrated in the silicate fraction and P_2O_5 in apatite.

The Al_2O_3/TiO_2 ratio of these mudstones varied in the order of 13–32. Hayashi $et\ al.$[25] suggested a Al_2O_3/TiO_2 ratio of 21–70 for felsic rocks when SiO_2 varies between 66 and 76 wt%. SiO_2 content of the studied mudstones ranges between 49 and 87 wt%, with an Al_2O_3/TiO_2 ratio of 13–32. This suggests considerable Ti-bearing mafic phases like biotite, chlorite and illmenite derived from basic and low-grade metamorphic rocks along with felsic rocks.

The SiO_2/Al_2O_3–Na_2O/K_2O diagram of Herron[26] reveals that most of the mudstone plots in the arkose to litharenite field, whereas in the SiO_2/Al_2O_3–Fe_2O_3/K_2O diagram of Pettijohn $et\ al.$[27], these rocks are classified as shale (Figure 4). Pettijohn's classification does not clearly distinguish greywacke from the litharenite compared to Herron's plot (Figure 4). Petrographic studies of Siwalik sandstones, in general, have less feldspar than rock fragments to classify them as arkose[1–5,8]. The extremely low Na_2O/K_2O ratio in mudstone puts our plots in the arkosic field (Figure 4 b), which indicates immaturity of the sediments. This is also supported by petrographic observation of Siwalik sandstone[1–5,8].

In the tectonic discrimination diagrams (Figure 5), after Roser and Korsch[28], and Maynard $et\ al.$[29], all the Siwalik mudstone samples plot in the passive margin field, although the Siwalik detritus is deposited in a dynamic fluvial setting. This suggests that the provenance signature always does not necessarily reflect the true depositional setting, but inherits the original source signature. Further, higher ratio of K_2O/Na_2O indicates significant input of potash from K-feldspar, illite and muscovite, thus modifying the chemical signature of the mudstone.

Weathering effect can be evaluated in terms of molecular percentage of the oxide components using the formula[9], CIA = $[Al_2O_3/(Al_2O_3+CaO*+Na_2O+K_2O)] \times 100$ in molecular proportion, where CaO* is the CaO associated with silicate fraction as opposed to that incorporated in the carbonates and phosphates. In the present study, total CO_2 content was not determined. Therefore, we cannot introduce correction for the carbonates to obtain true CaO*. To calculate CaO*, we have accepted that its value is ≤Na_2O; for CaO > Na_2O, concentration[30] of CaO is equal to that of Na_2O. This procedure provides a measure of the ratio of the secondary aluminous mineral to feldspar,
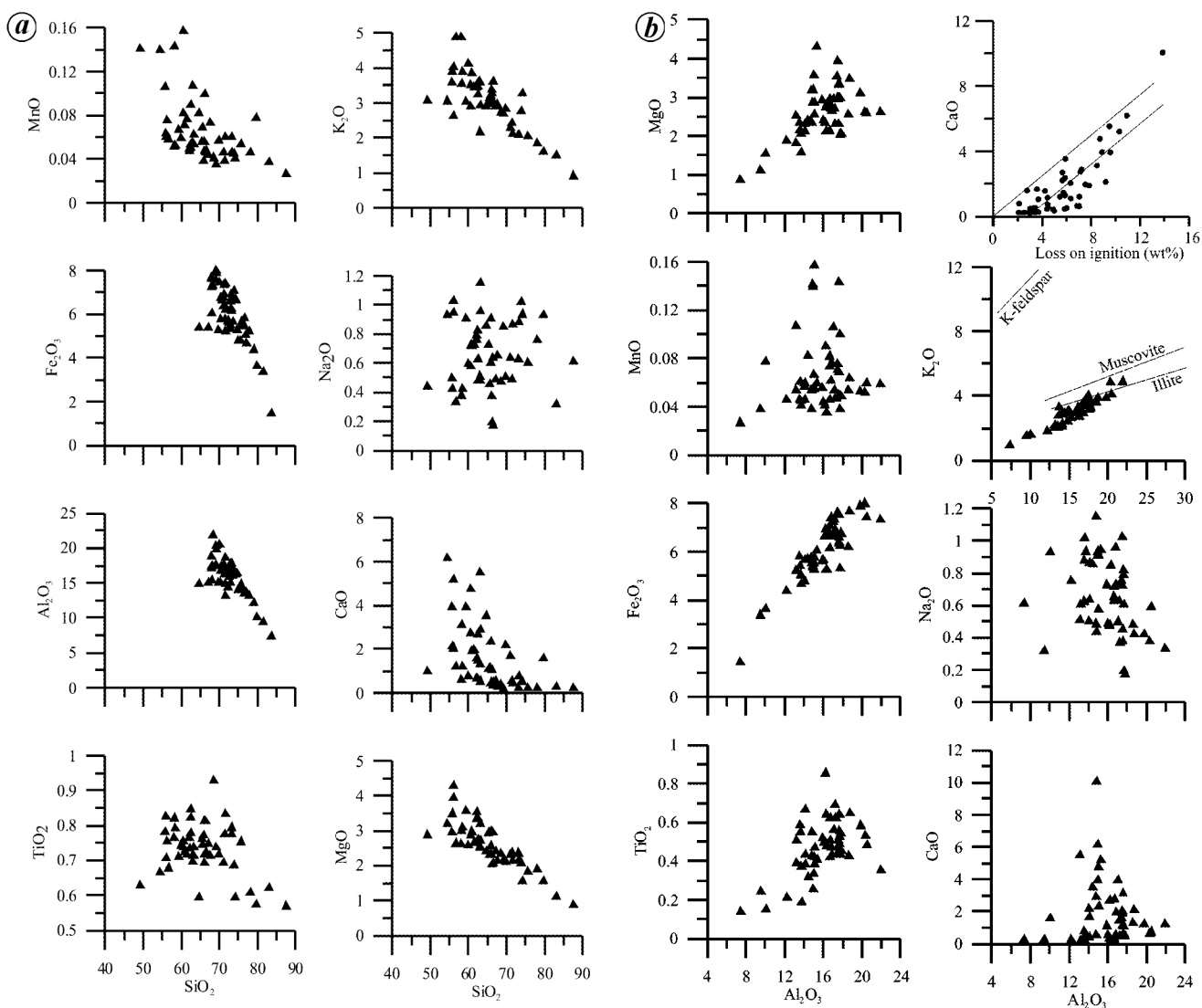
Figure 2. Major element chemical variations (in wt%) for the Katilu Khad mudstone samples with respect to SiO_2 (*a*) and Al_2O_3 (*b*).
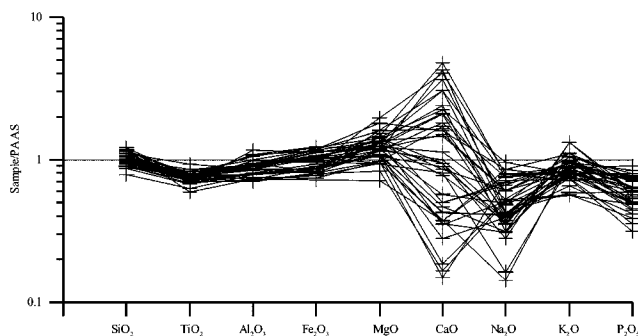

Figure 3. PAAS-normalized major oxide spider plot. Normalizing values after Nance and Taylor[16].

values of muscovite, illite and smectite, indicating contribution from a large proportion of clay minerals. Unweathered igneous rocks have values close to 50, whereas intensely weathered residual rocks forming kaolinite and gibbsite have values[9] approaching 100. This value in PAAS is reported to be 69, which is in agreement with those obtained from the mudstones of Punjab re-entrant in the present study, suggesting modest to high degree of chemical weathering. Since all the sediments were derived from the same source, compositional difference between the mudstones may have been controlled by different degrees of weathering (Figure 6).

Trace and rare earth elements

Due to remarkably high concentrations of trace elements in clay-rich sediments, most geochemical studies are focussed

and forms a basis for the measure of degree of weathering. The CIA computed for the mudstones have values ranging between 56.78 and 80.82 (average 75). CIA value for average shale[23] ranges from 70 to 75, which also reflects
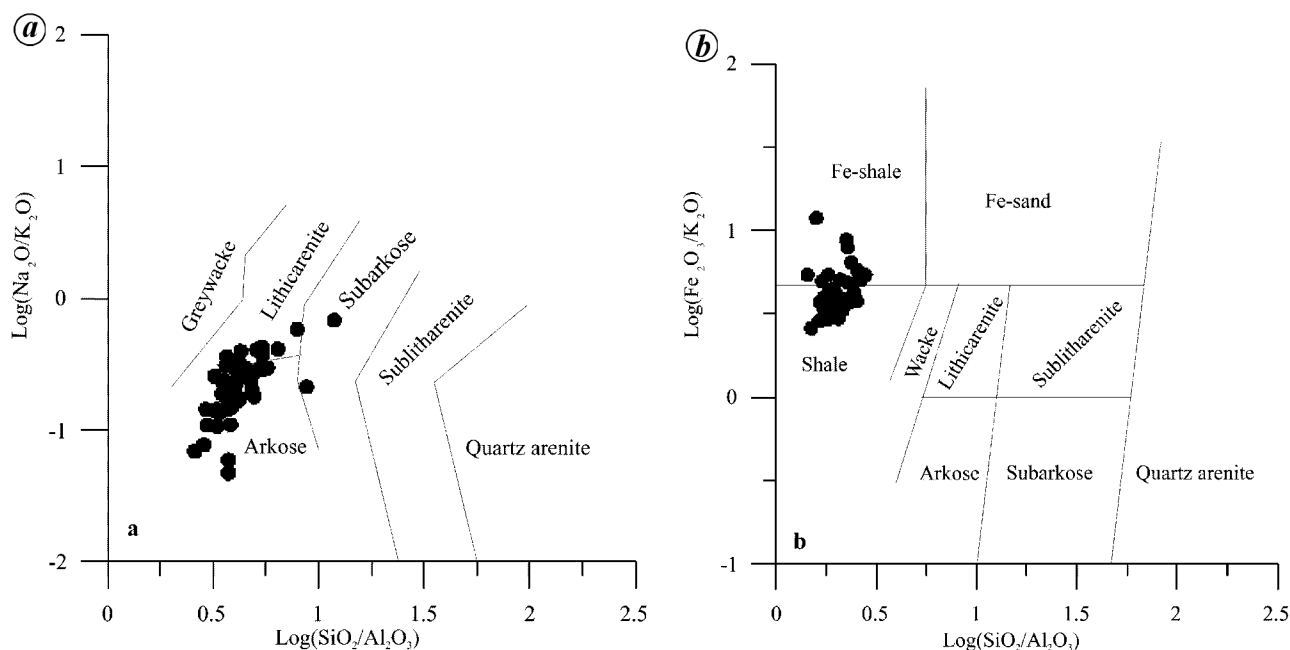
Figure 4. Plot of Katilu Khad mudstone samples on geochemical classification diagrams: (*a*) log (Na$_2$O/K$_2$O) vs log (SiO$_2$/Al$_2$O$_3$) after Herron[26], and (*b*) log (Fe$_2$O$_3$/K$_2$O) vs log (SiO$_2$/Al$_2$O$_3$) after Pettijohn *et al.*[27].
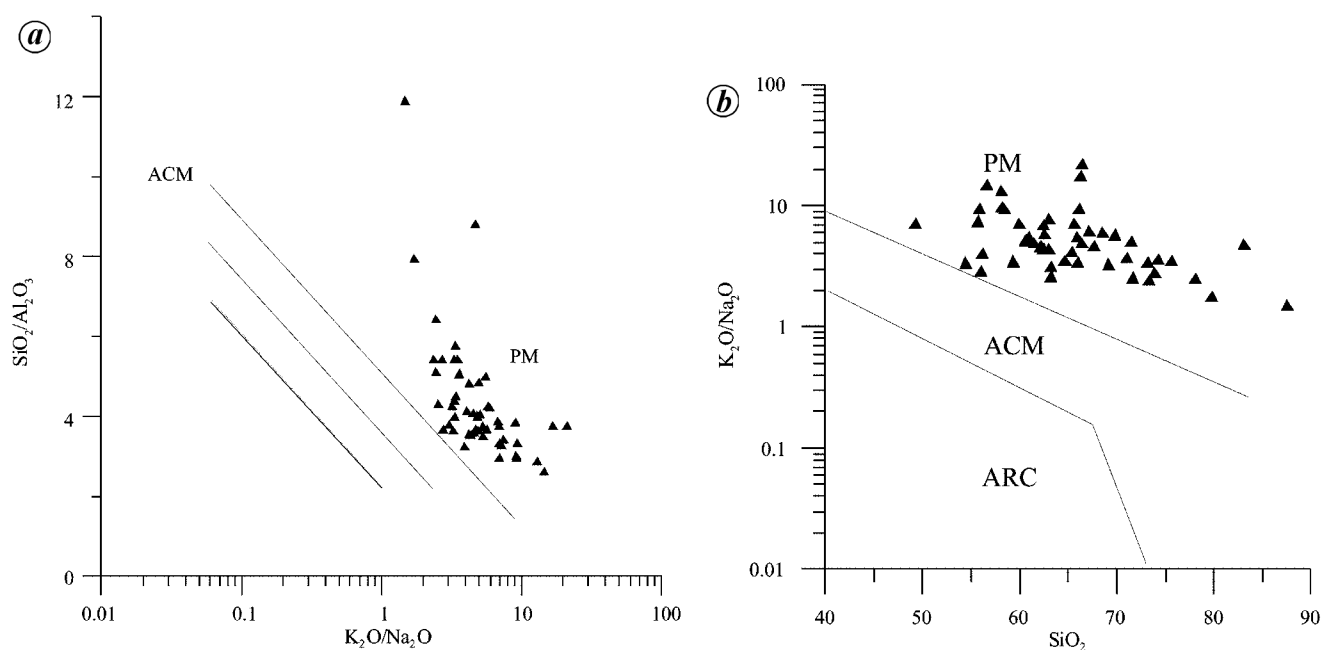
Figure 5. *a*, Tectonic discrimination diagram of Katilu Khad mudstone samples showing SiO$_2$/Al$_2$O$_3$–K$_2$O/Na$_2$O relationship. The provenance fields are after Roser and Korsch[28]. Mudstones samples plot in the passive margin PM field. ACM, Active continental margin field; ARC, Continental arc. *b*, Tectonic discrimination diagram after Maynard *et al.*[29], where K$_2$O/Na$_2$O ratio has been plotted with SiO$_2$ showing mudstones plot in PM field.

on these lithologies[16,31,32]. REEs, as well as Th, Sc, and to a lesser extent Cr and Co, are the most useful elements for provenance characterization, because they are among the least-soluble trace elements and are relatively immobile. These elements are believed to be transported exclu-

sively in terrigenous components of the sediment and therefore, reflect the chemistry of their source rocks[33,34].

The transition trace elements Cr and Ni are enriched and Co is depleted in the Siwalik mudstones compared to PAAS and show positive correlation with Al$_2$O$_3$. Enrichment

of Cr and Ni in these mudstones is either due to adsorption or substitution of these metals onto clay-size particles during weathering and deposition[35], or due to inputs from basic rock sources. The Mandi-Darla mafic volcanics located north of the study area, may be responsible for the relative enrichment of Cr and Ni. In the La–Th–Sc ternary diagram[36,37], majority of the samples fall in the field of granite-gneiss and metabasic mixed source (Figure 7), suggesting derivation from granite/gneiss and mafic rocks.
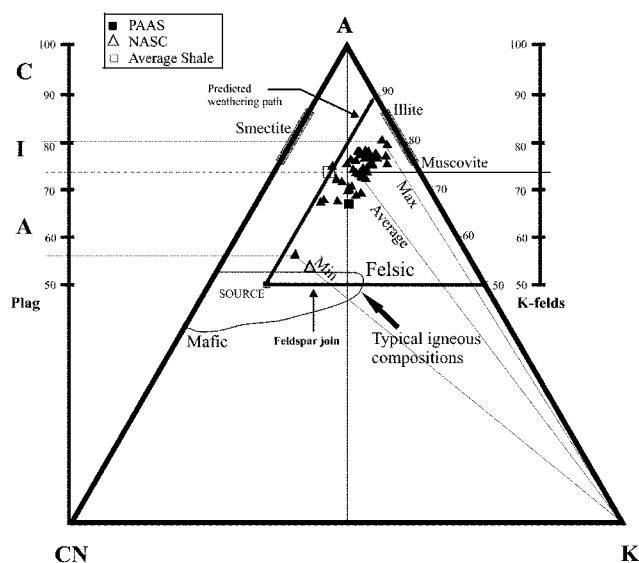
Figure 6. A–CN–K plots for Katilu Khad mudstone samples wherein mole fraction, A = Al_2O_3, C = CaO (silicate fraction only), N = Na_2O and K = K_2O. Most mudstone samples plot around the field of average shale[23], suggesting a moderate weathering history for the provenance.
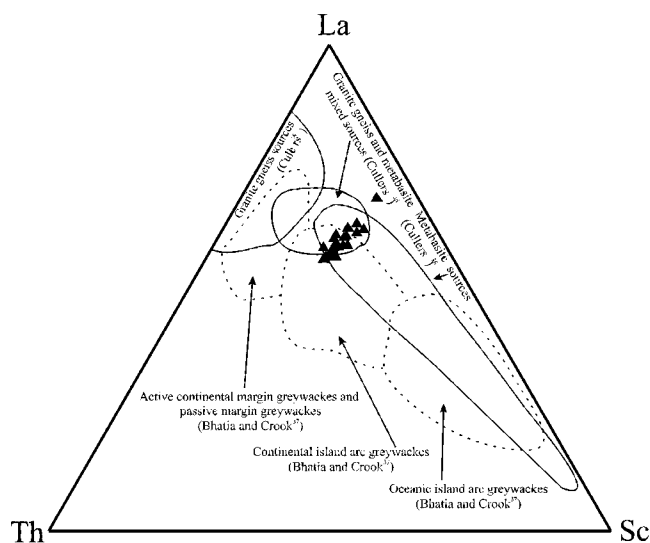
Figure 7. La–Th–Sc discriminating diagram for Katilu Khad mudstone. Compositional fields of greywacke from known tectonic settings and metamorphic sources of various composition are drawn for comparison.
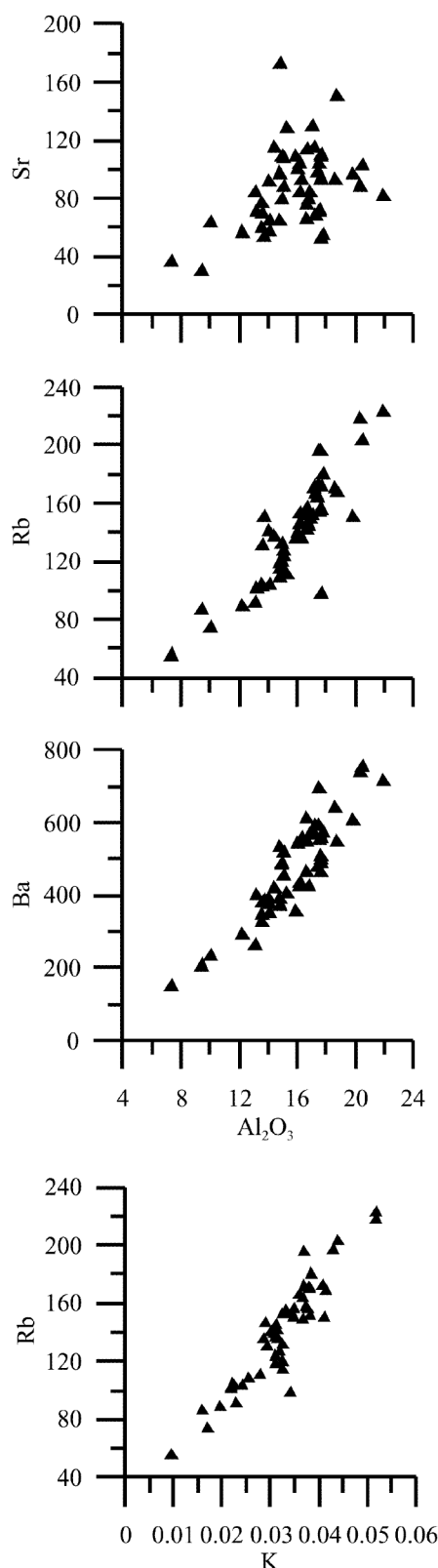
Figure 8. Bivariate plots of various trace elements depicting chemical variations for the mudstone samples. The positive correlation of Ba, Rb and Sr content of the Katilu Khad mudstones indicates a phyllosillicate-controlled distribution, whereas the positive correlation of K vs Rb in the mudstones indicates an alkali feldspar and illite clay control on these elements.
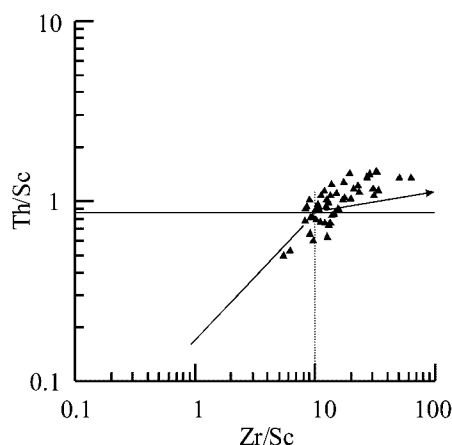
Figure 9. Plot of Th/Sc versus Zr/Sc for the selected Katilu Khad mudstone samples showing enrichment of zircon (high Zr/Sc ratio), fields of sedimentary recycling and compositional variations. Samples which are more affected show high Zr/Sc ratio and are interpreted as the sedimentary recycled, and those less affected are due to compositional variation of the provenance.
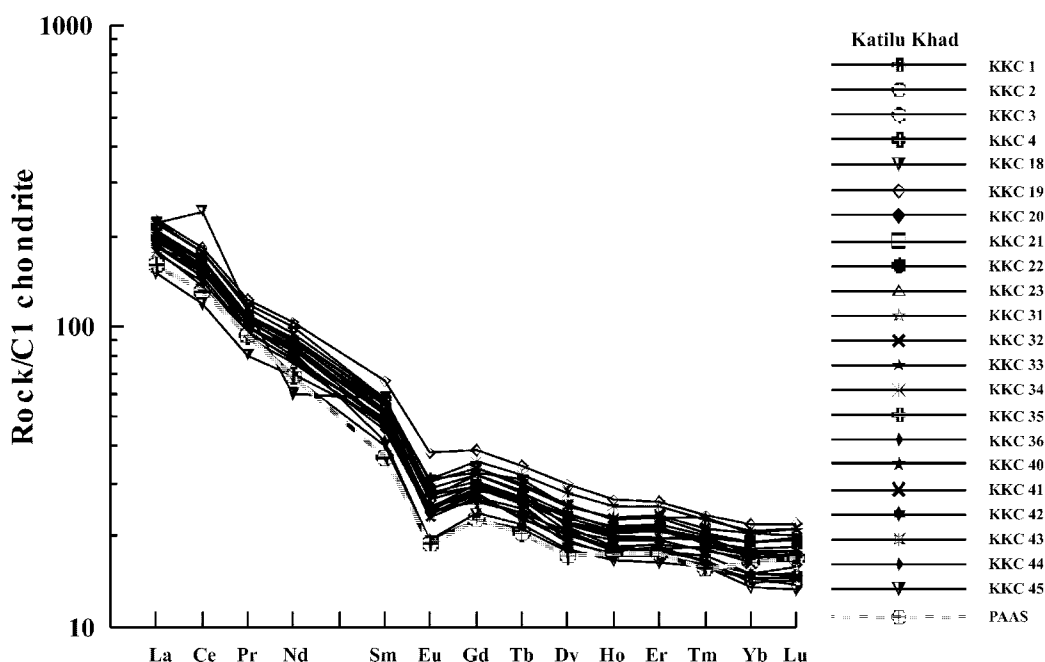

Figure 10. Chondrite-normalized average REE patterns of some selected samples of the Katilu Khad mudstones. Normalizing chondrite values are after Taylor and McLennan[23].

The Large Ion Lithophile Elements (LILE) like Rb, Ba and Sr are compared with PAAS. Among these, concentration of Rb is almost close to PAAS, but Sr and Ba are highly depleted. This suggests that the sediments have suffered weathering, erosion and re-depositional cycles which translocated these trace elements.

Rb, Ba and Sr, showing high positive correlation with Al_2O_3 (Figure 8), indicate that the distribution of these elements is controlled by phyllosilicates. The strong positive correlation of Rb with K (Figure 8) reveals its association with illitic phases, because Rb with respect to K, is preferentially retained in the illite during weathering processes[35,38]. This is because small cations such as Na,

Ca and Sr are selectively leached and removed from the weathering profiles, whereas cations with relatively larger ionic radii, such as K, Cs, Rb and Ba, may remain fixed by preferential exchange and adsorption on clays[35,38].

The high abundances of Zr (102–468 ppm) in these mudstones indicate that sediments were derived from zircon-enriched source rocks, such as two mica S-type Dhauladhar granite rocks, which show enrichment in Zr and Rb and strong depletion in Sr[39]. Zr/Sc is a useful index of zircon enrichment, since zircon is strongly enriched in Zr, whereas Sc is not enriched but still preserves a signature of the provenance[11]. Th/Sc is a good indicator of the igneous chemical differentiation process since Th is typically

an incompatible element, whereas Sc is compatible to the igneous systems[12]. The Th/Sc and Zr/Sc plot (Figure 9) of these mudstones suggests both compositional variations and new addition of Zr in the sedimentary system. Since Zr is concentrated in denser minerals like zircon, the Zr/Sc ratio provides a measure of sedimentary recycling and sorting[11]. Hence, the mudstones in the study area represent recycled components along with compositional variations. This signifies addition of zircon from weathered sources like phyllite, slate and mica-schist that are associated with the granitic material.

The chondrite-normalized REE patterns of analysed samples (Table 3) are shown in Figure 10. Mudstones show uniform REE patterns with LREE enrichment and a moderately flat HREE, suggesting the presence of heavy minerals like zircon[40,41]. The pattern also shows pronoun-
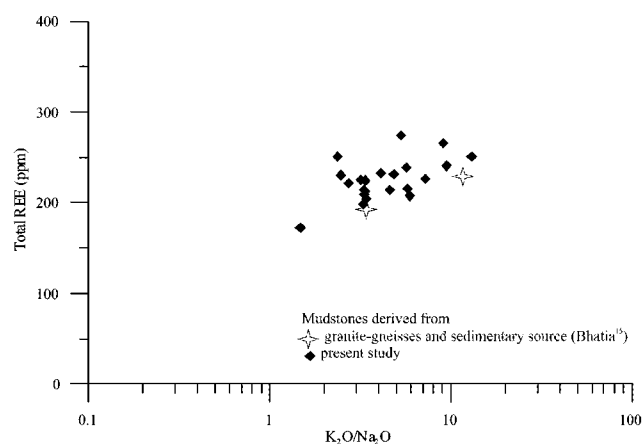
Figure 11. Total REE (in ppm) vs K_2O/Na_2O plot for Katilu Khad mudstones. Samples from known sources are plotted for comparison.
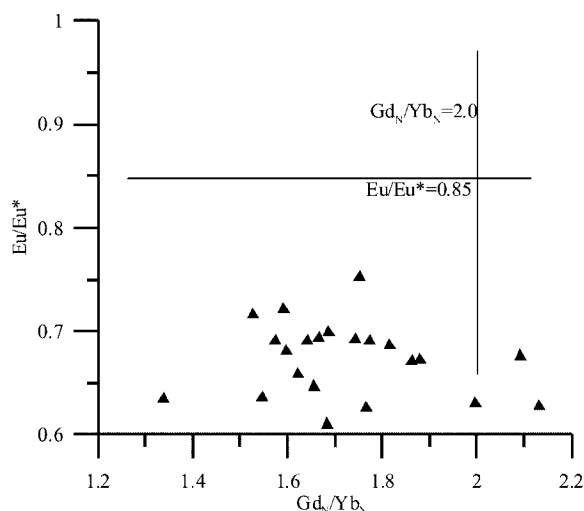
Figure 12. Plot of Eu/Eu* vs Gd_N/Yb_N for selected mudstone samples of Katilu Khad. Lower values of Eu/Eu* suggest that the igneous/metamorphic provenance was affected by intracrustal differentiation. Plot of majority of the samples shows that the sedimentary rocks were derived primarily from Phanerozoic sources from the Dhauladhar granitic massif.

ced negative Eu anomalies (Eu/Eu* = 0.61–0.75). This indicates sediment derived from an evolved crustal source. The general uniformity of REE pattern reveals that fractionation or alteration did not significantly affect the REE characteristics and reflects the original signature of the source. It is generally believed that the transport of REE into sedimentary basins is primarily a result of mechanical rather than chemical transport[16]. Therefore, uniformity of REE patterns in the mudstones suggest no significant redistribution of REE within weathering profiles[23]. The ΣREE vs K_2O/Na_2O ratio plot[15] (Figure 11) shows that the main sources for the sediments are granite-gneisses and sedimentary rocks possibly derived from the Lower Tertiary rocks, Chail Group of rocks and the Dhauladhar granite.

As discussed by McLennan[42], and Taylor and McLennan[23], the granitic rocks formed during Phanerozoic have more K-feldspar-rich granites and thereby reflect less depletion of Eu, and greater depletion of HREE with $Gd_N/Yb_N < 2$. The Eu/Eu* vs Gd_N/Yb_N plot (Figure 12) of the selected samples falls in the Phanerozoic field of granites having Gd_N/Yb_N ratio <2.0 except for KKC-2 (2.04) and KKC-4 (2.08). This suggests major contributions from the 500-Ma-old Phanerozoic Dhauladhar granite along with minor inputs from older 1400-Ma-old Baragaon mylonitic augen gneiss. High values of La_N/Sm_N (3.35–4.61), Ce_N/Yb_N (7.39–11.83), La_N/Yb_N (9.31–13.91) and depleted values of Gd_N/Yb_N (1.30–2.08) match well with those of felsic igneous rock or reworked sedimentary provenance (normalizing values from Evensen *et al.*[43]).

Conclusions

The geochemical signatures obtained from the mudstones of Punjab re-entrant indicate a mixed source composed of granite-gneiss (Dhauladhar granite and Baragaon gneiss), low-grade metamorphics (Lesser Himalayan), mafic (Mandi-Darla basic rocks) and sedimentary (Lower Tertiary) rocks.

The higher average value of CIA reveals modest to intense chemical weathering and possibly points to a humid climate in the source area. Th/Sc vs Zr/Sc ratio indicates that majority of the sediments are recycled. Prominent LREE enrichment and negative Eu anomaly suggest dominant granitic contribution over other lithologies.

This study reveals that the geochemical signature of Siwalik sediments can be used for deciphering the lithological composition, source-area weathering, provenance and tectonic setting of the basin. These geochemical parameters can also be used for source-basin modelling in future.

1. Tandon, S. K. and Rangaraj, S., In *Structural Geology of Himalaya* (ed. Saklani, P. S.), Today and Tomorrow's Printers and Publ., New Delhi, 1979, pp. 273–282.
2. Krynine, P. D., Petrography and genesis of the Siwalik series. *Am. J. Sci.*, 1937, **34**, 422–446.
3. Tandon, S. K., Siwalik sedimentation in a part of Kumaun Himalaya. *Sediment. Geol.*, 1976, **16**, 131–154.

4. Ghosh, S. K. and Kumar, R., Petrography of Neogene Siwalik sandstone of the Himalayan foreland basin, Garhwal Himalaya: Implications for source area tectonics and climate. *J. Geol. Soc. India*, 2000, **55**, 1–15.

5. Ghosh, S. K., Kumar, R. and Suresh, N., Influence of Mio-Pliocene drainage re-organization in the detrital modes of sandstone, Subathu sub-basin, Himalayan foreland basin. *J. Himalayan Geol.*, 2000, **324**, 35–46.

6. Kumar, R., Ghosh, S. K., Mazari, R. K. and Sangode, S. J., Tectonic impact on fluvial deposits of Plio-Pleistocene Himalayan foreland basin, India. *Sediment. Geol.*, 2003, **158**, 209–234.

7. Kumar, R., Ghosh, S. K. and Sangode, S. J., A multistorey sandstone complex in the Himalayan Foreland Basin, NW Himalaya, India. *J. Asian Earth Sci.*, 2004, **23**, 407–426.

8. Raiverman, V., Foreland sedimentation. In *Himalayan Tectonic Regime. A Relook at the Orogenic Process*, Bishen Singh Mahendra Pal Singh, Dehra Dun, 2002, p. 371.

9. Nesbitt, H. W. and Young, G. M., Early Proterozoic climates and plate motions inferred from major element chemistry of lutites. *Nature*, 1982, **299**, 715–717.

10. Cox, R., Lowe, D. R. and Cullers, R. L., The influence of sediment recycling and basement composition on evolution of mudrock chemistry in the southwestern United States. *Geochim. Cosmochim. Acta*, 1995, **59**, 2919–2940.

11. Basu, A., Petrology of Holocene fluvial sand derived from plutonic source rocks: implications of palaeoclimate interpretation. *J. Sediment. Petrol.*, 1976, **46**, 694–709.

12. McLennan, S. M., Hemming, S., McDaniel, D. K. and Hanson, G. N., Geochemical approaches to sedimenatation, provenance and tectonics. *Geol. Soc. Am. Spec. Pap.*, 1993, **285**, 21–40.

13. Cullers, R. L., Basu, A. and Suttner, L. J., Geochemical signature of provenance in sand-size material in soils and stream sediments near the Tobacco Root batholith, Mt, USA. *Chem. Geol.*, 1988, **70**, 335–348.

14. McLennan, S. M., Rare earth elements in sedimentary rocks: influences of provenance and sedimentary processes. *Rev. Mineral.*, 1989, **21**, 169–200.

15. Bhatia, M. R., Rare earth element geochemistry of Australian Paleozoic graywackes and mudrocks: Provenance and tectonic control. *Sediment. Geol.*, 1985, **45**, 97–113.

16. Nance, W. B. and Taylor, S. R., Rare earth element pattern and crustal evolution: I. Australian post-Archean sedimentary rocks. *Geochim. Cosmochim. Acta*, 1976, **40**, 1539–1551.

17. Thakur, V. C., Structure of the Chamba nappe and position of the Main Central Thrust in Kashmir Himalaya. *J. Asian Earth Sci.*, 1998, **16**, 269–282.

18. Bhanot, V. B., Geol., A. K., Singh, V. P. and Kwatra, S. K., Rb–Sr radiometric studies for the Dalhousie and Rohtang areas, Himachal Pradesh. *Curr. Sci.*, 1975, **44**, 219–220.

19. Mehta, P. K., Rb–Sr Geochronology of the Kulu–Mandi Belt, its implications for the Himalayan tectogenesis. *Geol. Rundsch.*, 1977, **66**, 156–175.

20. Islam, R., Upadhay, R., Ahmad, T., Thakur, V. C. and Sinha, A. K., Pan-African magmatism and sedimentation in the NW Himalaya. *Gondwana Res.*, 1999, **2**, 263–270.

21. Bhanot, V. B., Kwatra, S. K., Kansal, A. K. and Pandey, B. K., Rb–Sr whole rock age for Chail Series of northwestern Himalaya. *J. Geol. Soc. India*, 1978, **19**, 224–225.

22. Lucas-Tooth, H. and Pyne, C., *Advances in X-Ray Analysis*, Plenum Press, New York, 1964, vol. 7, p. 523.

23. Taylor, S. R. and McLennan, S. M., *The Continental Crust: Its Composition and Evolution*, Blackwell Scientific, Oxford, 1985, p. 312.

24. Lee, J. Il. and Lee, Yong Il, Geochemistry and provenance of Lower Cretaceous Sindong and Hayang mudrocks, Gyeongsang Basin, Southeastern Korea. *Geosci. J.*, 2003, **7**, 107–122.

25. Hayashi, K.-I., Fujisawa, H., Holland, H. D. and Ohmoto, H., Geochemistry of 1.9 Ga sedimentary rocks from northeastern Labrador, Canada. *Geochim. Cosmochim. Acta*, 1997, **61**, 4115–4137.

26. Herron, M. M., Geochemical classification of terrigenous sands and shales from core or log data. *J. Sediment. Petrol.*, 1988, **58**, 820–829.

27. Pettijohn, F. J., Potter, P. E. and Siever, R., In *Sand and Sandstone*, Springer-Verlag, New York, 1972, p. 618.

28. Roser, B. P. and Korsch, R. J., Determination of tectonic setting of sandstone–mudstone suites using SiO_2 content and K_2O/Na_2O ratio. *J. Geol.*, 1986, **94**, 635–650.

29. Maynard, J. B., Valloni, R. and Yu, H. S., In *Sedimentation and Tectonics on Modern and Ancient Active Plate Margins*, Blackwell Scientific, Oxford, 1982, pp. 551–561.

30. Bock, B., McLennan, S. M. and Hanson, G. N., Geochemistry and provenance of the Middle Ordovician Austin Glen Member (Normanskill Formation and the Taconian Orogeny in New England. *Sedimentology*, 1998, **45**, 635–655.

31. Andre, L., Deutsch, S. and Hertogen, J., Trace-element and Nd isotopes in shales as indexes of provenance and crustal growth: The early Paleozoic from the Brabant massif (Belgium). *Chem. Geol.*, 1986, **57**, 101–115.

32. Bhatia, M. R. and Taylor, S. R., Trace element geochemistry and sedimentary provinces: A study from the Tasman Geosyncline, Australia. *Chem. Geol.*, 1981, **33**, 115–125

33. Rollinson, H. R., *Using Geochemical Data: Evaluation, Presentation, Interpretation*, Longman, 1993, p. 352.

34. McLennan, S. M., Nance, W. B. and Taylor, W. B., Rare-earth element-thorium correlations in sedimentary rocks, and the composition of the continental crust. *Geochim. Cosmochim. Acta*, 1980, **44**, 1833–1839.

35. Wronkiewicz, D. J. and Condie, K. C., Geochemistry and provenance of sediments from the Pangola Supergroup, South Africa: Evidence for a 3.0 Ga-old continental craton. *Geochim. Cosmochim. Acta*, 1989, **53**, 1537–1549.

36. Cullers, R. L., The controls on the major- and trace-element evolution of shales, siltstones and sandstones of Ordovician to Tertiary age in the Wet Mountains region, Colorado, USA. *Chem. Geol.*, 1994, **113**, 327–343.

37. Bhatia, M. R. and Crook, A. W., Trace element characteristics of graywackes and tectonic setting discrimination of sedimentary basins. *Contrib. Mineral. Petrol.*, 1986, **92**, 181–193.

38. Nesbitt, H. W., Markovics, G. and Price, R. C., Processes affecting alkalis and alkaline earths during continental weathering processes. *Geochim. Cosmochim. Acta*, 1980, **44**, 1659–1666.

39. Mukherjee, P. K., Purohit, K. K., Rathi, M. S., Khanna, P. P., Saini, N. K. and Islam, R., Geochemistry and Petrogenesis of a Supracrustal Granite from Dalhousie, Himachal Himalaya. *J. Geol. Soc. India*, 1998, **52**, 163–180.

40. Cullers, R. L., The chemical signature of source rocks in size fractions of Holocene stream sediment derived from metamorphic rocks in the Wet Mountains region, Colorado, USA. *Chem. Geol.*, 1995, **123**, 107–131.

41. Ugidos, J. M., Armenteros, I. and Barba, P., Geochemistry of recycled orogen-derived sediments: a case study from Upper Precambrian siliciclastic rocks of the Central Iberian Zone, Iberian Massif, Spain. *Precambrian Res.*, 1997, **84**, 163–180.

42. McLennan, S. M., Petrological characteristics of Archean greywackes. *J. Sediment. Petrol.*, 1984, **54**, 889–898.

43. Evensen, N. M., Hamilton, P. J. and O'Nions, R. K., Rare earth element abundances in chondrite meteorites. *Geochim. Cosmochim. Acta*, 1978, **42**, 1199–1212.